

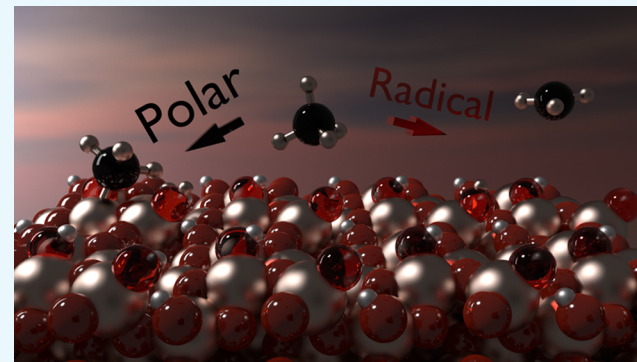
Computational Study of Methane Activation on $\gamma\text{-Al}_2\text{O}_3$

Mitchell C. Cholewinski,^{‡,†} Mudit Dixit,[†] and Giannis Mpourmpakis^{*}^{†,‡}

Department of Chemical Engineering, University of Pittsburgh, Pittsburgh, Pennsylvania 15261, United States

S Supporting Information

ABSTRACT: The C–H activation of methane remains a longstanding challenge in the chemical industry. Metal oxides are attractive catalysts for the C–H activation of methane due to their surface Lewis acid–base properties. In this work, we applied density functional theory calculations to investigate the C–H activation mechanism of methane on various sites of low-index facets of $\gamma\text{-Al}_2\text{O}_3$. The feasibility of C–H activation on different metal–oxygen (acid–base) site pairs was assessed through two potential mechanisms, namely, the radical and polar. The effect of surface hydroxylation on C–H activation was also investigated to examine the activity of $\gamma\text{-Al}_2\text{O}_3$ under realistic catalytic surface conditions (hydration). On the basis of our calculations, it was demonstrated that the C–H activation barriers for polar pathways are significantly lower than those of the radical pathways on $\gamma\text{-Al}_2\text{O}_3$. We showed that the electronic structure (s- and p-band center) for unoccupied and occupied bands can be used to probe site-dependent Lewis acidity and basicity and the associated catalytic behavior. We identified the dissociated H_2 binding and final state energy as C–H activation energy descriptors for the preferred polar pathway. Finally, we developed structure–activity relationships for the C–H activation of methane on $\gamma\text{-Al}_2\text{O}_3$ that account for surface Lewis acid–base properties and can be utilized to accelerate the discovery of catalysts for methane (and shale gas) upgrade.



INTRODUCTION

The recent development of hydraulic fracking technology and increasing shale gas reserves make natural gas an attractive feedstock for the synthesis of high-value chemicals.^{1–3} Direct combustion of methane cannot utilize its full potential in the chemical industry.⁴ Owing to the low volumetric density of methane, its transportation from rural-area shale reserves is expensive and challenging. Therefore, there is significant demand to convert methane to high-value and high-density chemicals. Currently, the transformation of methane in industry is achieved via an indirect process of its conversion to syn-gas ($\text{CO} + \text{H}_2$) at elevated temperatures (>970 K).^{5,6} However, this process is energetically demanding and cost-ineffective. Due to the high C–H bond strength of methane, an industrially viable process for the efficient and selective conversion of methane to higher value chemicals has yet to be realized. Interestingly, the conversion of methane (e.g., to methanol)^{1,7} is thermodynamically viable but kinetically challenging.^{1,7} Efficient and selective catalysts are required to overcome this kinetic difficulty. Metal oxides are known to catalyze reactions involving C–H activation^{8,9} because of their surface Lewis acid (metal) and base (oxygen) sites.^{8–15} Toward activating the C–H bond of methane, various metal oxides have been widely explored using experimental^{8,9} and computational^{9,16–24} methods. Interestingly, preheated $\gamma\text{-Al}_2\text{O}_3$ (at high temperature, >400 °C) is one of the most active catalysts for C–H activation of methane.^{25–27} Preheated $\gamma\text{-Al}_2\text{O}_3$ catalyzes the hydrogen–deuterium exchange reaction

of the mixture of D_2/CH_4 and CH_4/CD_4 at room temperature with very low activation barriers.^{25–27} It has been demonstrated that the thermal pretreatment of $\gamma\text{-Al}_2\text{O}_3$ generates high-energy surfaces, which are primarily responsible for the activity of $\gamma\text{-Al}_2\text{O}_3$ toward hydrogen–deuterium exchange.^{28,29} Recently, it was shown that preheated $\gamma\text{-Al}_2\text{O}_3$ (at 500 °C) shows exceptional activity for alkane C–H activation and dehydrogenation.³⁰ It is believed that the high-temperature pretreatment exposes under-coordinated surface acid–base site pairs.^{30–33} Valla et al. have demonstrated that the tricoordinated Al sites are generated by high-temperature pretreatment of $\gamma\text{-Al}_2\text{O}_3$.³⁴ Sautet and co-workers computationally studied the C–H activation of methane and propane on $\gamma\text{-Al}_2\text{O}_3$ (110) on several catalytic sites (e.g. $\text{Al}^{\text{III}}\text{-O}^{\text{II}}$ and $\text{Al}^{\text{III}}\text{-O}^{\text{III}}$) through the polar pathway.^{31,32,35,36} The authors also investigated the effect of surface hydration on methane activation on these sites. C–H activation of methane can potentially occur through the polar^{16–18} or radical mechanism.^{22,37–39} In the polar mechanism, a C–H bond of methane breaks heterolytically to form surface-bound hydroxyl and methyl-aluminum species. The radical mechanism evolves through the homolytic C–H bond cleavage with the formation of radical intermediates. In this mechanism, the hydrogen radical reacts with surface oxygen to form surface hydroxyl and releases the

Received: September 27, 2018

Accepted: December 12, 2018

Published: December 26, 2018

methyl radical in the gas phase. It has been suggested that the radical pathway is usually favored in oxidative C–H activation through oxygen-centered radicals or on doped metal oxides.^{39,40} However, the feasibility of radical pathway has not been assessed on $\gamma\text{-Al}_2\text{O}_3$ yet.

Due to the high surface heterogeneity of oxides (existence of various sites with variable Lewis acidity and basicity), the identification of structure–activity relationships (relationships between the catalyst properties and reaction activity) is highly desirable. These relationships offer a rational understanding of catalytic activity and a predictive tool for discovering and designing active catalysts.^{41–43} Toward the identification of structure–activity relationships, Latimer et al. recently established the adsorption energy of atomic hydrogen as universal oxidative C–H activation descriptor through the radical pathway.¹⁹ Recently, Jiang et al. investigated C–H activation of methane on oxygen atoms, which were preadsorbed on Co_3O_4 and identified the Adjusted Coordination Number (based on generalized coordination number and Bader charges) as a descriptor for the C–H activation barrier.²³ Janik and co-workers revealed a correlation between the C–H bond activation energy and the surface reducibility.²¹ As a result, significant research has been focused on oxidative C–H activation of methane on single (oxygen) site over the last few decades, but the nonoxidative C–H activation of methane on oxides (on acid–base pair sites) remains underexplored. In addition, there is no systematic approach to screen oxide catalysts toward a catalytic reaction. The key hurdle, which possibly hinders the development of structure–activity relationships for nonoxidative C–H activation, is the existence of a large number of inequivalent sites with variable Lewis acidity/basicity (high surface heterogeneity) on the oxides.⁴⁴ In the nonoxidative C–H activation, both Lewis acid and base sites are involved in the reaction at the same time, and probing these properties on oxide surfaces with variable coordination environments (affecting Lewis acidity and basicity) becomes significantly complex.⁴⁵ In our recent work, we developed structure–activity relationships for propane dehydrogenation on $\gamma\text{-Al}_2\text{O}_3$ that unraveled the dependence of the propane dehydrogenation activity on the strength of surface acid–base site pairs. Moreover, we observed a site-dependent catalytic behavior of $\gamma\text{-Al}_2\text{O}_3$ and revealed a volcano relationship between activity and dissociated H₂ binding energy (BE) on the respective site pairs.⁴⁶

In this work, we focus on methane activation on $\gamma\text{-Al}_2\text{O}_3$ because of its high degree of surface heterogeneity^{45,47,48} and high catalytic activity. These properties make $\gamma\text{-Al}_2\text{O}_3$ an excellent candidate to identify structure–activity relationships for nonoxidative C–H activation. Specifically, we applied first-principles calculations to identify the preferred mechanism of C–H activation on different low-index surface facets of $\gamma\text{-Al}_2\text{O}_3$, by also accounting surface hydration. Our work revealed structure–activity relationships for C–H activation of methane, which can be used for screening different metal oxides and aid in accelerated catalyst discovery.

RESULTS AND DISCUSSION

We employed the nonspinel model of alumina, as developed by Sautet and co-workers.^{47,48} Figure 1 shows the unit cell of $\gamma\text{-Al}_2\text{O}_3$ and different surface terminations (surface cleaving).

To examine the influence of Lewis acidity and basicity on the C–H activation barriers, we investigated the polar mechanisms on three low-index surface facets of $\gamma\text{-Al}_2\text{O}_3$:

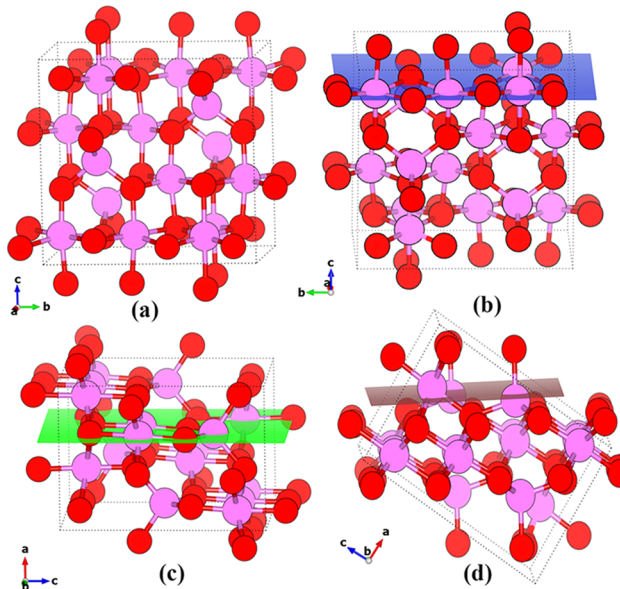


Figure 1. Structure of $\gamma\text{-Al}_2\text{O}_3$ (a) bulk, (b) (100) (blue), (c) (110) (green), and (d) (111) (brown) termination planes.

(100), (110), and (111), as shown in Figure 2.^{47,48} These surface facets of $\gamma\text{-Al}_2\text{O}_3$ were optimized, and it was noticed

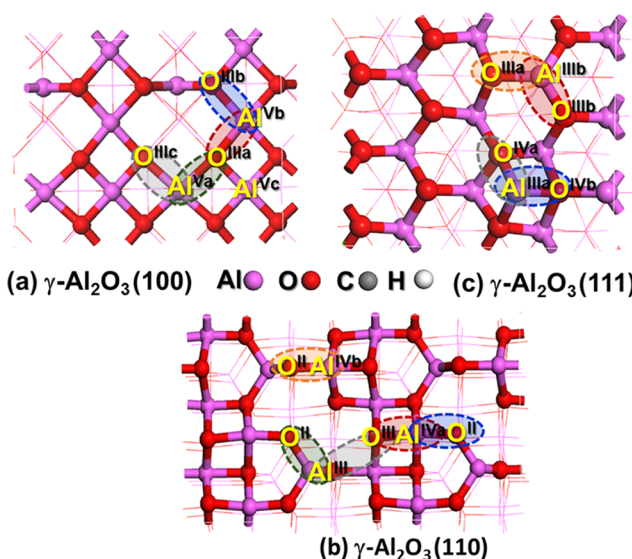


Figure 2. Top view of the different metal–oxygen site pairs on $\gamma\text{-Al}_2\text{O}_3$ (a) (100), (b) (110), and (c) (111) surface facets.

that Al atoms display pentacoordination (Al^{V}) on (100) facet, tetra- (Al^{IV}) and tricoordinations (Al^{III}) on (110) facet, and tricoordination (Al^{III}) on (111) facet. Oxygen atoms were found to display tricoordination (O^{III}) on $\gamma\text{-Al}_2\text{O}_3$ (100) facet, di- (O^{II}) and tricoordinations (O^{III}) on (110) facet, and tri- (O^{III}) and tetracoordinations (O^{IV}) on (111) facet.^{47,48} We choose different distinctive acid–base site pairs (based on the coordination numbers) on each surface facet (Figure 2). Specifically, the selected site pairs are: on $\gamma\text{-Al}_2\text{O}_3$ (100) facet, $\text{Al}^{\text{Vb}}-\text{O}^{\text{IIIa}}$, $\text{Al}^{\text{Vb}}-\text{O}^{\text{IIIa}}$, $\text{Al}^{\text{Vb}}-\text{O}^{\text{IIIb}}$, $\text{Al}^{\text{Va}}-\text{O}^{\text{IIIc}}$, on $\gamma\text{-Al}_2\text{O}_3$ (110) facet, $\text{Al}^{\text{III}}-\text{O}^{\text{II}}$, $\text{Al}^{\text{III}}-\text{O}^{\text{III}}$, $\text{Al}^{\text{IVa}}-\text{O}^{\text{II}}$, $\text{Al}^{\text{IVa}}-\text{O}^{\text{III}}$ and $\text{Al}^{\text{IVb}}-\text{O}^{\text{II}}$, and on $\gamma\text{-Al}_2\text{O}_3$ (111) facet, $\text{Al}^{\text{IIIa}}-\text{O}^{\text{IVa}}$, $\text{Al}^{\text{IIIa}}-\text{O}^{\text{IVb}}$, $\text{Al}^{\text{IIIb}}-\text{O}^{\text{IIIa}}$ and $\text{Al}^{\text{IIIb}}-\text{O}^{\text{IIIb}}$.

The electronic structure of the catalyst plays an important role on the overall catalytic activity.^{49,50} To understand the Lewis acidity and basicity of different sites of $\gamma\text{-Al}_2\text{O}_3$, we investigated the projected density of states of the (100), (110), and (111) facets of $\gamma\text{-Al}_2\text{O}_3$. For molecular systems, the locations of the highest occupied molecular orbital and lowest unoccupied molecular orbital, are related with the Lewis acidity (electrophilicity) and basicity (nucleophilicity) of these systems, as these orbitals are involved in electron loss and gain processes, respectively.⁵¹ By analogy, for periodic surfaces, the Lewis acidity and basicity can be probed by identifying the location of the centers of unoccupied and occupied bands, respectively. Toward assessing the Lewis acidity and basicity of different site pairs, we calculated the projected density of states Al(s) and O(p) orbitals of $\gamma\text{-Al}_2\text{O}_3$ (100), (110), and (111) facets (Figure 3). It is clear from Figure 3 that low-lying

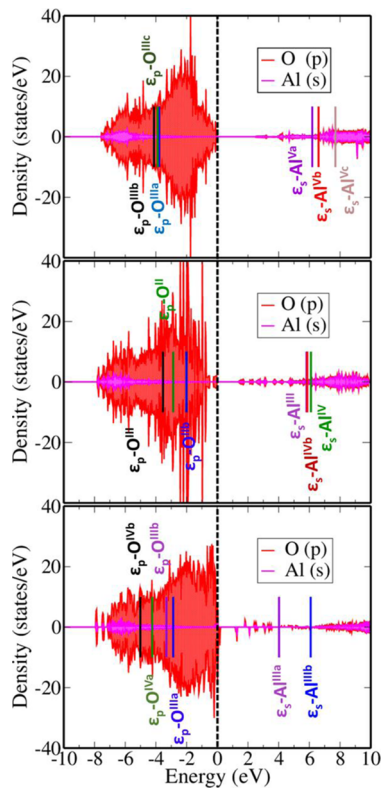


Figure 3. Projected density of states of Al(s) and O(p) states of (top panel) (100), (middle panel) (110), and (bottom panel) (111) facet of $\gamma\text{-Al}_2\text{O}_3$. Locations of s- and p-band centers are shown with vertical lines. The calculated values of s- and p-band centers are given in Table S1. Fermi level was shifted to zero.

unoccupied bands of aluminum atoms are Al(s) bands, and high-lying occupied bands of oxygen atoms are O(p) bands. Therefore, we computed the unoccupied s-band center (ϵ_s^{Al}) for Al atoms and occupied p-band center (ϵ_p^{O}) of O atoms. On the (100) facet, based on the unoccupied s-band center the Lewis acidity of aluminum atoms follows the trend (lower ϵ_s = more acidic): Al^{Va} ($\epsilon_s = 6.19$) > Al^{Vb} ($\epsilon_s = 6.6$) > Al^{Vc} ($\epsilon_s = 7.71$). This trend is in agreement with previous calculations by Jenness et al.⁵² The calculated occupied p-band center suggests that the Lewis basicity of oxygen atoms on the (100) facet follows the trend: O_{IIIa} ($\epsilon_p = -3.78$) $\approx \text{O}_{\text{IIIc}}$ ($\epsilon_p = -3.89$) > O_{IIb} ($\epsilon_p = -4.13$). On the (110) facet, the strongest Lewis acid site is Al^{III} ($\epsilon_s = 5.81$) followed by Al^{IVb} ($\epsilon_s = 5.87$) site,

and the weakest Lewis acid site is Al^{IVa} ($\epsilon_s = 6.11$). The basicity of oxygen atoms bound with Al^{IVa} follows the order of O^{II} ($\epsilon_p = -2.87$) > O^{III} ($\epsilon_p = -3.53$). On the (111) facet, the strongest Lewis acid site is Al^{IIIa} ($\epsilon_s = 4.03$) followed by Al^{IIIb} ($\epsilon_s = 6.09$).

After assessing the site-dependent Lewis acidity and basicity, we turn our attention to the C–H activation mechanisms of methane. In general, there are two potential surface mechanisms that exist for C–H activation of methane on oxide catalysts, the polar and radical pathways.^{16–18,37} The former mechanism is characterized by polar (heterolytic) dissociation of C–H bond of methane, whereas the latter is characterized by homolytic dissociation of the C–H bond of methane. The polar mechanism (Figure 4, top panel) involves the C–H bond breaking of methane in heterolytic fashion on the surface to yield CH_3^* and surface-adsorbed H^{+*} . In the radical mechanism (Figure 4, bottom panel), the C–H bond breaks by the abstraction of a hydrogen radical by a surface oxygen atom while leaving a methyl radical in the gas phase. To investigate the effects of Lewis acidity and basicity on C–H activation of methane, we examined both mechanisms on two stable facets ((100) and (110)) of $\gamma\text{-Al}_2\text{O}_3$. Additionally, the polar mechanism was also investigated on the (111) facet of Al_2O_3 . Figure 4 illustrates the relevant stationary points in both pathways, radical and polar on the $\text{Al}^{\text{Va}}\text{-O}^{\text{IIIa}}$ site pair.

Initially, we investigated the polar mechanism on the four acid–base site pairs ($\text{Al}^{\text{Va}}\text{-O}^{\text{IIIa}}$, $\text{Al}^{\text{Vb}}\text{-O}^{\text{IIIb}}$, $\text{Al}^{\text{Va}}\text{-O}^{\text{IIIc}}$, and $\text{Al}^{\text{Vb}}\text{-O}^{\text{IIIa}}$) of (100) facet (Figure 2a), the five site pairs ($\text{Al}^{\text{III}}\text{-O}^{\text{II}}$, $\text{Al}^{\text{IVa}}\text{-O}^{\text{II}}$, $\text{Al}^{\text{IVa}}\text{-O}^{\text{III}}$, $\text{Al}^{\text{Vb}}\text{-O}^{\text{II}}$, and $\text{Al}^{\text{III}}\text{-O}^{\text{III}}$) of the (110) facet (Figure 2b), and the four site pairs ($\text{Al}^{\text{IIIa}}\text{-O}^{\text{IVa}}$, $\text{Al}^{\text{IIIa}}\text{-O}^{\text{IVb}}$, $\text{Al}^{\text{IIIb}}\text{-O}^{\text{IIIa}}$, and $\text{Al}^{\text{IIIb}}\text{-O}^{\text{IIIb}}$) of the (111) facet (Figure 2c). We noticed that adsorption of methane is weakly exothermic on the (100) and (110) facets, and it becomes stronger on the (111) facet due to low average surface coordination numbers of Al and oxygen atoms on this facet. For the polar mechanism on the (100) facet (Figure 5a), the lowest C–H activation barrier was obtained on the site pair with strongest Lewis acidity and basicity ($\text{Al}^{\text{Va}}\text{-O}^{\text{IIIa}}$, 94.5 kJ/mol) followed by the site pair involving the strongest acidic site ($\text{Al}^{\text{Va}}\text{-O}^{\text{IIIc}}$, 115 kJ/mol). The barriers on $\text{Al}^{\text{Vb}}\text{-O}^{\text{IIIb}}$ (174.2 kJ/mol) and $\text{Al}^{\text{Vb}}\text{-O}^{\text{IIIa}}$ (141.6) sites pairs are found relatively higher due to lower acidity/basicity of corresponding acid–base pairs. On the (110) facet (Figure 5b), low C–H activation barriers (84–91 kJ/mol) were obtained on the site pairs with strong Lewis acidity and basicity ($\text{Al}^{\text{III}}\text{-O}^{\text{II}}$ and $\text{Al}^{\text{IVb}}\text{-O}^{\text{II}}$). However, the C–H activation was highly exothermic on the $\text{Al}^{\text{III}}\text{-O}^{\text{II}}$ site pair, demonstrating the strong Lewis acidity and basicity of corresponding atoms of the site pairs. On this facet, the highest activation barrier was noted for site pair with high surface coordination numbers ($\text{Al}^{\text{IVa}}\text{-O}^{\text{III}}$, 126.8 kJ/mol). On the (111) facet (Figure 5c), lowest C–H activation barriers (64.4 and 66.6 kJ/mol) were noted for the $\text{Al}^{\text{IIIa}}\text{-O}^{\text{IVa}}$ and $\text{Al}^{\text{IIIa}}\text{-O}^{\text{IVb}}$ site pairs. The activity behavior on these site pairs might appear counter intuitive (due to high coordination number of oxygen), however, due to the involvement of strongest Lewis acidic ($\epsilon_s = 4.03$) site, these site pairs display low C–H activation barriers.

Next, we investigated the radical mechanism on the two most stable facets of $\gamma\text{-Al}_2\text{O}_3$, the (100) and (110). The (111) facet was not considered for the radical pathway as this (nonhydrated) facet is higher in energy, and it has been experimentally demonstrated that the (111) facet is present in low content on $\gamma\text{-Al}_2\text{O}_3$ particles.^{53,54} Specifically, we

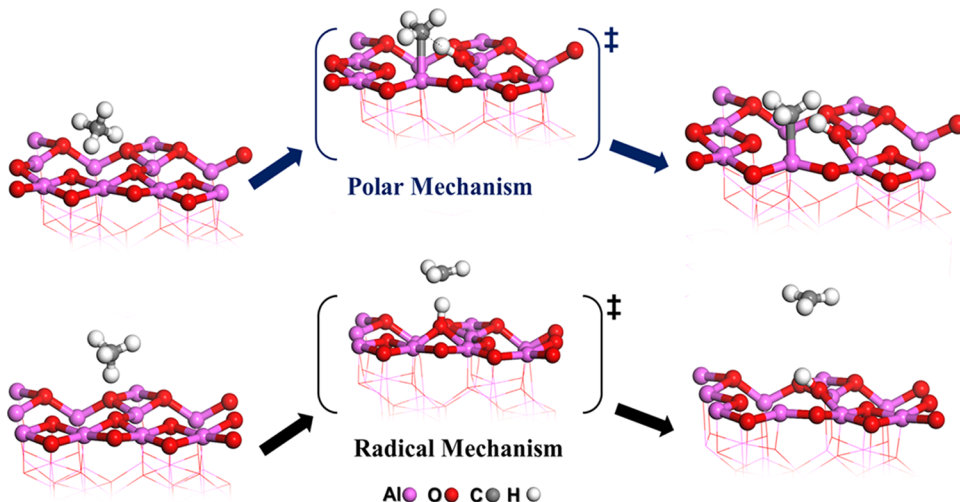


Figure 4. Polar and radical mechanisms of C–H activation of methane on $\gamma\text{-Al}_2\text{O}_3$ (100) on the $\text{Al}^{\text{Va}}-\text{O}^{\text{IIIa}}$ site pair. Transition states are denoted with double daggers (\ddagger). The top panel illustrates the polar mechanism, whereas the bottom, the radical.

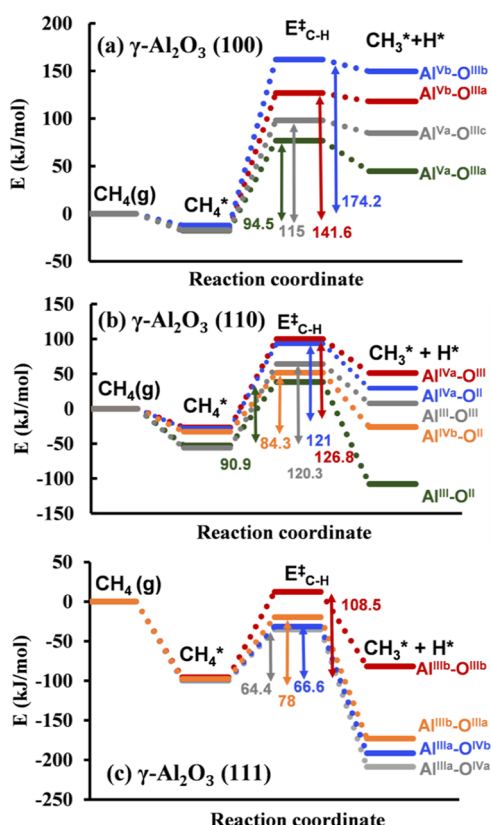


Figure 5. Methane C–H activation energy profiles on $\gamma\text{-Al}_2\text{O}_3$ (a) (100), (b) (110), and (c) (111) facets via the polar pathway. The respective site pairs are shown in Figure 2.

investigated the radical mechanism on two oxygen sites (O^{IIIa} and O^{IIIb}) of (100) facet and three oxygen sites O^{IIa} (O^{II} site of $\text{Al}^{\text{III}}-\text{O}^{\text{II}}$ site pair), O^{IIIa} (O^{III} site of $\text{Al}^{\text{IVa}}-\text{O}^{\text{III}}$ site pair), O^{IIb} (O^{II} site of $\text{Al}^{\text{IVb}}-\text{O}^{\text{II}}$ site pair) on the (110) facet.

To investigate the radical pathways, we started with closed shell (singlet) calculations on (100) facet. All attempts to find the transition state with singlet calculations failed. In these calculations, the guess geometry for the final state converges to the initial states. Furthermore, the potential energy scan along the C–H bond coordinate also indicated a highly endothermic

(uphill) path (Figure S2). Subsequently, we investigated the radical pathway with triplet states and successfully identified potential transition states. However, the triplet reactant states for adsorbed methane were found to be significantly higher in energy compared to corresponding singlet states (Figure 6).

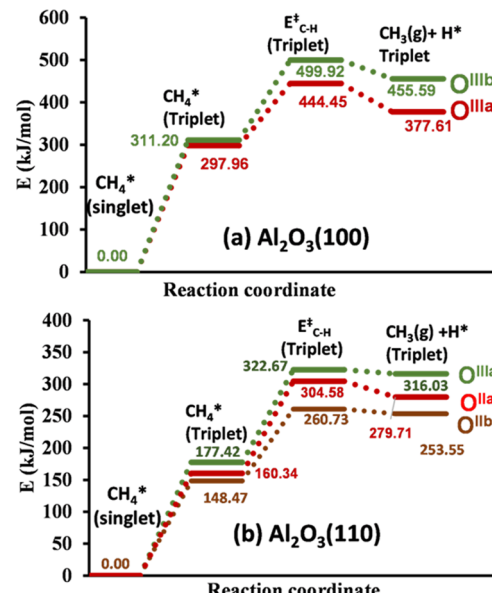


Figure 6. Methane C–H activation energy profiles on $\gamma\text{-Al}_2\text{O}_3$ (a) (100) and (b) (110) facets via the radical pathway. The O^{IIa} site corresponds to the O^{II} site of the $\text{Al}^{\text{III}}-\text{O}^{\text{II}}$ site pair, the O^{IIb} site corresponds to the O^{II} site of the $\text{Al}^{\text{IVb}}-\text{O}^{\text{II}}$ site pair, and the O^{IIIa} site on 110 facet corresponds to the O^{III} site of the $\text{Al}^{\text{IVa}}-\text{O}^{\text{III}}$ site pair. The respective sites are shown in Figure 2.

The C–H activation barriers for radical pathways were found to be highly endothermic for both the (100) and (110) facets investigated in this work. We note that the C–H barriers via radical pathways on the (110) facet are lower than that of the (100) facet.

As already discussed, we observed significantly dissimilar C–H activation barriers on site pairs with different Lewis acidities and basicities (surface coordination) on the various surface facets of $\gamma\text{-Al}_2\text{O}_3$. To further probe the Lewis acidity and

basicity, we calculated the binding energies of dissociated H_2 ($\text{BE}-\text{H}_2$) on all of the different site pairs of (100), (110), and (111) facets. The choice of $\text{BE}-\text{H}_2$ as a Lewis acidity/basicity descriptor is based on the fact that the adsorptions of hydride and proton (on the corresponding metal and oxygen sites) resulting from the dissociated hydrogen ($\text{H}_2 \rightarrow \text{H}^+ + \text{H}^-$) act as an effective probe for both electron-rich (oxygen) and electron-deficient (aluminum) atoms. Additionally, in our recent work, we identified the binding energy of dissociated H_2 as an activity descriptor for nonoxidative propane dehydrogenation on $\gamma\text{-Al}_2\text{O}_3$.⁵⁵ By plotting the $\text{BE}-\text{H}_2$ against the respective activation barriers for the most preferred, i.e., polar mechanism (Figure 7a), we verify that it is a good

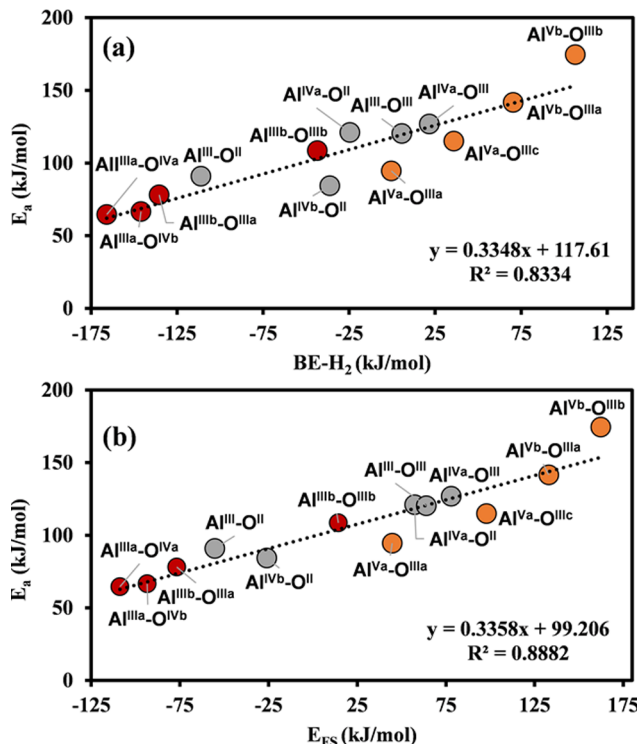


Figure 7. Methane C–H activation barriers on $\gamma\text{-Al}_2\text{O}_3$ for polar mechanism vs (a) dissociated H_2 binding energies and (b) final state energy with respect to adsorbed state of methane, on the corresponding acid–base sites. Orange points represent sites on (100), gray on (110), and red on (111) facets of $\gamma\text{-Al}_2\text{O}_3$.

descriptor of methane C–H activation energy. In addition, a well-known descriptor for C–H activation is the final state energy, E_{FS} ^{20,56,57} (difference in energy between the physisorbed and final (activated) states of methane on the catalyst surface). This descriptor is based on BEP-type relationships^{58–60} (due to the late transition state of C–H activation). We plotted the final state energy vs the activation energy of C–H activation of methane through the polar pathway, and we noted a good correlation as well (Figure 7b). Taken together, these suggest that the binding energy of hydrogen and the final state energy can be used as interchangeable descriptors for the C–H activation of methane. The identified descriptors (Figure 7) relate the catalyst activity with reactant–catalyst physicochemical properties and thus can be used for the construction of structure–activity relationships. Interestingly, by plotting the dissociated H_2 binding energies on different site pairs of (100) and (111)

facets vs the difference between occupied s-band center of Al and occupied p-band center of O, we revealed a good correlation (Figure S3). This finding demonstrates a quantitative relationship between band centers and Lewis acidity and basicity.

Under realistic experimental conditions, the Lewis acid surface sites (under-coordinated Al sites) of $\gamma\text{-Al}_2\text{O}_3$ are partially occupied by hydroxyl groups, and some of the Lewis basic surface sites (oxygen atoms) are protonated due to surface hydration. Computational work established that the fully nonhydroxylated (100) facet is more stable than that of nonhydroxylated (110) facet,^{50,58} and the presence of hydroxyl groups significantly stabilizes the (110) facet, making it the most abundant facet.^{47,48,61} As a result, to assess the activity of $\gamma\text{-Al}_2\text{O}_3$ under realistic experimental conditions, we investigated the effect of hydroxylation of $\gamma\text{-Al}_2\text{O}_3$ (110) (most abundant facet) on methane activation. Previous studies by Digne and co-workers^{47,48} demonstrated that the (110) facet of $\gamma\text{-Al}_2\text{O}_3$ has a hydroxyl coverage of $\sim 5.9 \text{ OH/nm}^{-2}$ at temperatures 700–950 K (within typical nonoxidative alkane dehydrogenation conditions). Therefore, we consider eight hydroxylated configurations of $\gamma\text{-Al}_2\text{O}_3$ (110) facet with a hydroxyl coverage of $\sim 5.9 \text{ OH/nm}^{-2}$ (i.e. four H_2O molecules per supercell). In the considered configurations, different surface sites were hydroxylated, and different surface oxygen atoms were protonated. We note that in the most stable hydroxylated configuration, the strongest Lewis acid sites (Al^{III} and Al^{IVb}) are now blocked by hydroxyl groups (Figure S4a), suggesting that these sites become inactive for methane activation.

In addition, it has been suggested that high-temperature pretreatment of $\gamma\text{-Al}_2\text{O}_3$ (activation) can expose defect Al^{III} sites that belong to metastable hydrated surfaces.^{31,32} Sautet and co-workers extensively studied the surface hydration of $\gamma\text{-Al}_2\text{O}_3$ and identified two types of metastable surface hydration models that expose a free Al^{III} site, namely, Digne's model (nonreconstructed) and Wischert model (reconstructed).^{31,32} Therefore, we considered two metastable structures with a free Al^{III} site (strong Lewis acid) for studying the CH_4 activation. Out of the two lowest energy metastable structures, the nonreconstructed structure, which is generated by the hydroxylation of one Al^{IVa} and Al^{III} site (Digne's model,⁴⁷ Figure S4b) and the protonation of O^{II} sites (Figure S4b) was found to be 76 kJ/mol higher in energy than the most stable structure. This surface configuration does not show any reconstruction. Interestingly, we note that on the $\text{Al}^{\text{III}}-\text{O}^{\text{III}}$ site pair, depending on the orientation of methane in the transition state, two distinct modes of C–H activation exist (Figure S5) because the nonadjacent acid–base sites involved in this pair are separated by a large distance. These two C–H activation modes are identified on the $\text{Al}^{\text{III}}-\text{O}^{\text{III}}$ site pair of both hydrated and nonhydrated surfaces. We note that the low-energy C–H activation mode (Figure S5) has a transition state with methane in a tetrahedral-like orientation (Figure S5a–c), whereas in the high-energy mode methane has a distorted geometry ($\text{S}_{\text{N}2}$ -like transition state geometry, Figure S5d–f). The distorted structure increases the energy at the transition state (due to strain).

The C–H activation barriers of the low-energy mode are presented in Figure 8. Reaction profiles for high-energy transition state modes are presented in Figure S6. On the $\text{Al}^{\text{III}}-\text{O}^{\text{II}}$ (adjacent) site pair of the nonreconstructed metastable hydroxylated configuration, the C–H activation

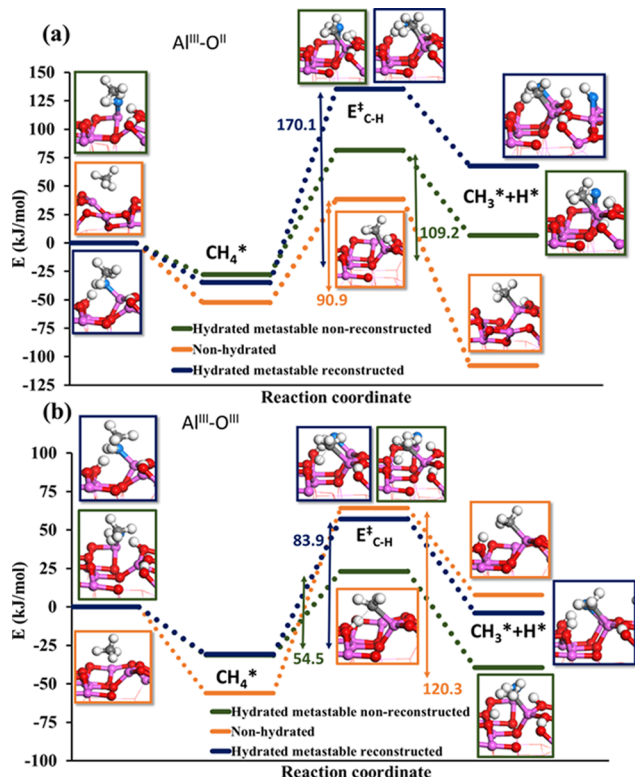


Figure 8. Methane C–H activation energy profiles (polar pathway) on (a) $\text{Al}^{\text{III}}-\text{O}^{\text{II}}$ and (b) $\text{Al}^{\text{III}}-\text{O}^{\text{III}}$ site pairs of nonhydrated and two metastable hydrated (110) $\gamma\text{-Al}_2\text{O}_3$ surfaces.

barrier (109.2 kJ/mol, Figure 8a) was found to be higher than that of the C–H activation barrier on the $\text{Al}^{\text{III}}-\text{O}^{\text{II}}$ site pair of nonhydrated configuration (90.9 kJ/mol, Figure 8a). On the $\text{Al}^{\text{III}}-\text{O}^{\text{III}}$ (nonadjacent) site pair of nonreconstructed metastable hydrated configuration, the C–H activation barrier (54.5 kJ/mol, Figure 8b) was found to be lower than that on $\text{Al}^{\text{III}}-\text{O}^{\text{III}}$ site pair of the nonhydrated configuration (120.3 kJ/mol, Figure 8b). These results are in agreement with previous reports^{31,32} where it was suggested that in the presence of bridging hydroxyl groups on Al^{IVa} , the activity of the $\text{Al}^{\text{III}}-\text{O}^{\text{III}}$ site pair increases due to the increase in the basicity of the O atom. The higher C–H activation barrier on the $\text{Al}^{\text{III}}-\text{O}^{\text{II}}$ of nonreconstructed hydrated surface can be attributed to the decrease in basicity of O^{II} site due to hydrogen bond (in 1.53 Å distance) with the hydrogen atom bound to the O^{II} site of the $\text{Al}^{\text{IVa}}-\text{O}^{\text{II}}$ site pair. The other considered hydrated metastable model (Figure S4c) of $\gamma\text{-Al}_2\text{O}_3$ (110), generated by the hydroxylation of both Al^{IVa} site and the protonation of less basic O^{III} site of $\text{Al}^{\text{IVb}}-\text{O}^{\text{III}}$ site pair (Figure S4c), reconstructed, in agreement with the previous results by Wischert et al.^{31,32} This reconstructed surface is lower in energy (by -47 kJ/mol) than of the nonreconstructed surface, but it was found to be higher in energy (by 29 kJ/mol) than the most stable hydrated surface. On the $\text{Al}^{\text{III}}-\text{O}^{\text{II}}$ (adjacent) site pair of the reconstructed hydrated surface, the C–H activation barrier (170.1 kJ/mol, Figure 8a) was found to be significantly higher than that of the C–H activation barrier on the $\text{Al}^{\text{III}}-\text{O}^{\text{II}}$ site pair of the nonhydrated surface (90.9 kJ/mol, Figure 8a). This increase in the barrier on the hydrated reconstructed facet is likely due to the change in coordination of O^{II} from dicoordinated to tricoordinated and modification of Al^{III} acidity due to reconstruction. This change in Lewis

acidity basicity of this site pair in the reconstructed metastable configuration is demonstrated by the higher final state energy of methane dissociation on this site pair (Figure 8a) when compared to that of the corresponding nonreconstructed metastable hydrated and nonhydrated site pairs. On the $\text{Al}^{\text{III}}-\text{O}^{\text{III}}$ (nonadjacent) site pair of reconstructed hydrated configuration, the C–H activation barrier (83.9 kJ/mol, Figure 8b) was found to be lower than that of the C–H activation barrier on the $\text{Al}^{\text{III}}-\text{O}^{\text{III}}$ site pair of nonhydrated configuration (120.3 kJ/mol, Figure 8b). The aforementioned results clearly demonstrate that the surface hydration can significantly influence the C–H activation barriers of methane by modifying the surface Lewis acidity and basicity. The low methane activation barrier (54.5 kJ/mol, Figure 8b) obtained on a nonadjacent site pair of metastable surface (generated through high-temperature pretreatment) rationalizes the experimentally observed high activity of thermally pretreated $\gamma\text{-Al}_2\text{O}_3$.^{28–30} Moreover, previously demonstrated activity poisoning of thermally preheated alumina by water can be explained by blocking of the defect active sites (such as $\text{Al}^{\text{III}}-\text{O}^{\text{III}}$ site on metastable surfaces) by strong water adsorption.^{28,30} Finally, we note that the final state energy can also be used as a descriptor for methane activation barriers on hydroxylated metastable surfaces (Figure S7).

CONCLUSIONS

We applied density functional theory (DFT) to investigate the C–H activation of methane on different sites of three low-index surface facets of $\gamma\text{-Al}_2\text{O}_3$. Two potential C–H activation mechanisms were considered on different sites of varying Lewis acidity and basicity, the polar and radical mechanism. It was found that the polar is the prevailing C–H activation mechanism on $\gamma\text{-Al}_2\text{O}_3$. We show that the site-dependent Lewis acidity and basicity can be probed by identifying the band centers for the unoccupied and occupied bands. Moreover, we address the effect of surface hydration on C–H activation of methane and show a modification of the Lewis acid/base properties and C–H activation behavior. Water generally blocks strong Lewis acid/base site pairs (catalytic suppression), but in some cases it can enhance activity of adjacent sites on metastable $\gamma\text{-Al}_2\text{O}_3$ surfaces. Importantly, we demonstrate that hydrogen dissociative binding energy and final state energy can be used as descriptors for the C–H activation on $\gamma\text{-Al}_2\text{O}_3$. These descriptors can be used in the construction of structure–activity relationships for C–H activation of methane and effectively probe the Lewis acid/base functionality of the metal oxide catalysts.

METHODS

The DFT calculations were performed using the CP2K program package.⁶² The Perdew–Burke–Ernzerhof (PBE) exchange-correlation functional⁶³ with Grimme’s D3 dispersion correction method⁶⁴ was used. TZVP basis sets were used for C, H, and O, and DZVP basis set was used for Al. Goedecker, Teter, and Hutter pseudopotentials were employed with a kinetic energy cutoff of 500 Ry. The minimum energy pathways for C–H activation were investigated using climbing image nudged elastic band calculations as implemented in CP2K.⁶⁵ The nonspinel model of alumina was used in our calculations.^{47,48} To model the (110), (100), and (111) facets of $\gamma\text{-Al}_2\text{O}_3$, $p2 \times 1$, $p1 \times 2$ and $p1 \times 1$ supercells were used (Figure S1), respectively. Supercells with 80 atoms were used

for (100) and (111) surfaces, and 120-atom supercell was used for (110) facet. For the radical pathway, the supercells with 160 atoms were used for both (110) and (100) facets (to locate transition states with the correct localization of spin) with a kinetic energy cutoff of 400 Ry. The two bottom layers were kept frozen at their corresponding bulk positions, and remaining layers were allowed to relax. The systems were relaxed using the forces and SCF convergence criterion of $4.0 \times 10^{-4} E_h$ per bohr and 10^{-7} au, respectively. The binding energy (BE) of hydrogen atoms was computed, by dissociative hydrogen adsorption on Lewis acid and base sites of the oxide surface, according to eq 1

$$BE_{H_2} = E_{\text{surface}/H_2} - (E_{H_2} + E_{\text{surface}}) \quad (1)$$

Where E_{surface/H_2} is the total energy of a H_2 adsorbed on the surface, E_{surface} and E_{H_2} are total energies of the clean surface and gas-phase H_2 , respectively. For the electronic structure analysis (e.g., density of states), DFT calculations with PBE functional were performed using the Vienna ab initio simulation package.^{66–68} Projector augmented wave pseudo-potentials and $3 \times 3 \times 3$ and $6 \times 6 \times 1$ k -points were used for bulk and surface calculations, respectively, with 520 eV kinetic energy cutoff. The unoccupied s-band center of Al (ϵ_s^{Al}) and occupied p-band center of O (ϵ_p^{O}) are defined as

$$\epsilon_s^{\text{Al}} = \frac{\int_{E_F}^{\infty} \rho_s^{\text{Al}}(\epsilon) \epsilon \, d\epsilon}{\int_{E_F}^{\infty} \rho_s^{\text{Al}}(\epsilon) \, d\epsilon} \quad \text{and} \quad \epsilon_p^{\text{O}} = \frac{\int_{-\infty}^{E_F} \rho_p^{\text{O}}(\epsilon) \epsilon \, d\epsilon}{\int_{-\infty}^{E_F} \rho_p^{\text{O}}(\epsilon) \, d\epsilon}$$

where E_F is the Fermi energy, ρ_s^{Al} and ρ_p^{O} are the PDOS of Al(s) and O(p), and ϵ is the energy (in eV).

■ ASSOCIATED CONTENT

S Supporting Information

The Supporting Information is available free of charge on the ACS Publications website at DOI: [10.1021/acsomega.8b02554](https://doi.org/10.1021/acsomega.8b02554).

Structure of surface facets of γ - Al_2O_3 ; band centers of aluminum and oxygen atoms and structures of hydrated γ - Al_2O_3 (110) surfaces; selected transition states for methane activation; C–H activation energy profiles on the $\text{Al}^{\text{III}}\text{–O}^{\text{III}}$ site pair of nonhydrated and hydrated (110) γ - Al_2O_3 and relationship between Lewis acidity/basicity and electron density band centers ([PDF](#))

■ AUTHOR INFORMATION

Corresponding Author

*E-mail: gmpourmp@pitt.edu.

ORCID

Mudit Dixit: [0000-0001-9456-7806](https://orcid.org/0000-0001-9456-7806)

Giannis Mpourmpakis: [0000-0002-3063-0607](https://orcid.org/0000-0002-3063-0607)

Present Address

[†]Health, Human Performance, and Recreation, Baylor University, Waco, Texas 76706, United States (M.C.C.).

Author Contributions

M.C.C and M.D. performed all of the theoretical calculations. G.M. conceptualized the study, and both G.M. and M.D. carried out the advising. All authors contributed to the preparation of the manuscript.

Author Contributions

[†]M.C.C. and M.D. contributed equally to this work.

Notes

The authors declare no competing financial interest.

■ ACKNOWLEDGMENTS

Acknowledgment is made to the Donors of the American Chemical Society Petroleum Research Fund (ACS-PRF) for support of this research. Computational support was provided by the Center for Research Computing at the University of Pittsburgh, and the Extreme Science and Engineering Discovery Environment, which is supported by the NSF (ACI-1053575).

■ REFERENCES

- (1) Tang, P.; Zhu, Q.; Wu, Z.; Ma, D. Methane activation: the past and future. *Energy Environ. Sci.* **2014**, *7*, 2580–2591.
- (2) Schwach, P.; Pan, X.; Bao, X. Direct Conversion of Methane to Value-Added Chemicals over Heterogeneous Catalysts: Challenges and Prospects. *Chem. Rev.* **2017**, *117*, 8497–8520.
- (3) Kerr, R. A. Natural Gas From Shale Bursts Onto the Scene. *Science* **2010**, *328*, 1624–1626.
- (4) McFarland, E. Unconventional chemistry for unconventional natural gas. *Science* **2012**, *338*, 340–342.
- (5) York, A. P. E.; Xiao, T.; Green, M. L. H. Brief Overview of the Partial Oxidation of Methane to Synthesis Gas. *Top. Catal.* **2003**, *22*, 345–358.
- (6) Choudhary, T. V.; Choudhary Vasant, R. Energy-Efficient Syngas Production through Catalytic Oxy-Methane Reforming Reactions. *Angew. Chem., Int. Ed.* **2008**, *47*, 1828–1847.
- (7) Gesser, H. D.; Hunter, N. R.; Prakash, C. B. The direct conversion of methane to methanol by controlled oxidation. *Chem. Rev.* **1985**, *85*, 235–244.
- (8) Sattler, J. J. H. B.; Ruiz-Martinez, J.; Santillan-Jimenez, E.; Weckhuysen, B. M. Catalytic Dehydrogenation of Light Alkanes on Metals and Metal Oxides. *Chem. Rev.* **2014**, *114*, 10613–10653.
- (9) Coperet, C. C–H Bond Activation and Organometallic Intermediates on Isolated Metal Centers on Oxide Surfaces. *Chem. Rev.* **2010**, *110*, 656–680.
- (10) Bañares, M. A. Supported Metal Oxide and Other Catalysts for Ethane Conversion: a Review. *Catal. Today* **1999**, *51*, 319–348.
- (11) McFarland, E. W.; Metiu, H. Catalysis by Doped Oxides. *Chem. Rev.* **2013**, *113*, 4391–4427.
- (12) Michorczyk, P.; Ogonowski, J. Dehydrogenation of Propane in the Presence of Carbon Dioxide Over Oxide-Based Catalysts. *React. Kinet. Catal. Lett.* **2003**, *78*, 41–47.
- (13) Nakagawa, K.; Okamura, M.; Ikenaga, N.; Suzuki, T.; Kobayashi, T.; et al. Dehydrogenation of Ethane Over Gallium Oxide In The Presence of Carbon Dioxide. *Chem. Commun.* **1998**, *9*, 1025–1026.
- (14) Kazansky, V. B.; Subbotina, I. R.; Pronin, A. A.; Schlogl, R.; Jentoft, F. C. Unusual Infrared Spectrum of Ethane Adsorbed by Gallium Oxide. *J. Phys. Chem. B* **2006**, *110*, 7975–7978.
- (15) Liu, Y.; Li, Z. H.; Lu, J.; Fan, K.-N. Periodic Density Functional Theory Study of Propane Dehydrogenation over Perfect $\text{Ga}_2\text{O}_3(100)$ Surface. *J. Phys. Chem. C* **2008**, *112*, 20382–20392.
- (16) Weaver, J. F.; Hakanoglu, C.; Antony, A.; Asthagiri, A. Alkane activation on crystalline metal oxide surfaces. *Chem. Soc. Rev.* **2014**, *43*, 7536–7547.
- (17) Liang, Z.; Li, T.; Kim, M.; Asthagiri, A.; Weaver, J. F. Low-temperature activation of methane on the $\text{IrO}_2(110)$ surface. *Science* **2017**, *356*, 299–303.
- (18) Antony, A.; Asthagiri, A.; Weaver, J. F. Pathways and kinetics of methane and ethane C–H bond cleavage on $\text{PdO}(101)$. *J. Chem. Phys.* **2013**, *139*, No. 104702.
- (19) Latimer, A. A.; Kulkarni, A. R.; Aljama, H.; Montoya, J. H.; Yoo, J. S.; Tsai, C.; Abild-Pedersen, F.; Studt, F.; Nørskov, J. K. Understanding trends in C–H bond activation in heterogeneous catalysis. *Nat. Mater.* **2016**, *16*, 225–229.

- (20) Latimer, A. A.; Aljama, H.; Kakekhani, A.; Yoo, J. S.; Kulkarni, A.; Tsai, C.; Garcia-Melchor, M.; Abild-Pedersen, F.; Norskov, J. K. Mechanistic insights into heterogeneous methane activation. *Phys. Chem. Chem. Phys.* **2017**, *19*, 3575–3581.
- (21) Kumar, G.; Lau, S. L. J.; Krcha, M. D.; Janik, M. J. Correlation of Methane Activation and Oxide Catalyst Reducibility and Its Implications for Oxidative Coupling. *ACS Catal.* **2016**, *6*, 1812–1821.
- (22) Krcha, M. D.; Mayernick, A. D.; Janik, M. J. Periodic trends of oxygen vacancy formation and C–H bond activation over transition metal-doped CeO₂ (1 1 1) surfaces. *J. Catal.* **2012**, *293*, 103–115.
- (23) Fung, V.; Tao, F. F.; Jiang, D.-e. General Structure–Reactivity Relationship for Oxygen on Transition-Metal Oxides. *J. Phys. Chem. Lett.* **2017**, *8*, 2206–2211.
- (24) Fung, V.; Polo-Garzon, F.; Wu, Z.; Jiang, D.-e. Exploring perovskites for methane activation from first principles. *Catal. Sci. Technol.* **2018**, *8*, 702–709.
- (25) Robertson, P. J.; Scurrell, M. S.; Kemball, C. Exchange of alkanes with deuterium over gamma-alumina. A Bronsted linear free energy relationship. *J. Chem. Soc., Faraday Trans. 1* **1975**, *71*, 903–912.
- (26) Hargreaves, J. S. J.; Hutchings, G. J.; Joyner, R. W.; Taylor, S. H. A study of the methane–deuterium exchange reaction over a range of metal oxides. *Appl. Catal., A* **2002**, *227*, 191–200.
- (27) Quanzhi, L.; Amenomiya, Y. Exchange reaction of methane on some oxide catalysts. *Appl. Catal.* **1986**, *23*, 173–182.
- (28) Weller, S. W.; Hindin, S. G. The Effect of Pretreatment on the Activity of Gamma-Alumina. II. Hydrogen–Deuterium Exchange. *J. Phys. Chem.* **1956**, *60*, 1506–1512.
- (29) Pines, H.; Ravoire, J. Alumina: Catalyst and support. xii. The effect of intrinsic acidity of Aluminas upon hydrogen-deuterium exchange. *J. Phys. Chem.* **1961**, *65*, 1859–1861.
- (30) Rodemerck, U.; Kondratenko, E. V.; Otroshchenko, T.; Linke, D. Unexpectedly High Activity of Bare Alumina for Non-Oxidative Isobutane Dehydrogenation. *Chem. Commun.* **2016**, *52*, 12222–12225.
- (31) Wischert, R.; Copéret, C.; Delbecq, F.; Sautet, P. Optimal Water Coverage on Alumina: A Key to Generate Lewis Acid–Base Pairs that are Reactive Towards the C–H Bond Activation of Methane. *Angew. Chem., Int. Ed.* **2011**, *50*, 3202–3205.
- (32) Wischert, R.; Laurent, P.; Copéret, C.; Delbecq, F.; Sautet, P. γ -Alumina: The Essential and Unexpected Role of Water for the Structure, Stability, and Reactivity of “Defect” Sites. *J. Am. Chem. Soc.* **2012**, *134*, 14430–14449.
- (33) Peri, J. B. Infrared Study of Adsorption of Carbon Dioxide, Hydrogen Chloride, and Other Molecules on “Acid” Sites on Dry Silica—Alumina and γ -Alumina. *J. Phys. Chem.* **1966**, *70*, 3168–3179.
- (34) Valla, M.; Wischert, R.; Comas-Vives, A.; Conley, M. P.; Verel, R.; Copéret, C.; Sautet, P. Role of Tricoordinate Al Sites in CH₃ReO₃/Al₂O₃ Olefin Metathesis Catalysts. *J. Am. Chem. Soc.* **2016**, *138*, 6774–6785.
- (35) Joubert, J.; Delbecq, F.; Sautet, P. Alkane Metathesis by a Tungsten Carbyne Complex Grafted on Gamma Alumina: Is There a Direct Chemical Role of the Support? *J. Catal.* **2007**, *251*, 507–513.
- (36) Joubert, J.; Salameh, A.; Krakoviack, V.; Delbecq, F.; Sautet, P.; Copéret, C.; Basset, J. M. Heterolytic Splitting of H₂ and CH₄ on γ -Alumina as a Structural Probe for Defect Sites. *J. Phys. Chem. B* **2006**, *110*, 23944–23950.
- (37) Lunsford, J. H. The catalytic oxidative coupling of methane. *Angew. Chem., Int. Ed.* **1995**, *34*, 970–980.
- (38) Krcha, M. D.; Janik, M. J. Examination of oxygen vacancy formation in Mn-doped CeO₂ (111) using DFT + U and the hybrid functional HSE06. *Langmuir* **2013**, *29*, 10120–10131.
- (39) Schwarz, H. Chemistry with methane: concepts rather than recipes. *Angew. Chem., Int. Ed.* **2011**, *50*, 10096–10115.
- (40) Aljama, H.; Norskov, J. K.; Abild-Pedersen, F. Theoretical Insights into Methane C–H Bond Activation on Alkaline Metal Oxides. *J. Phys. Chem. C* **2017**, *121*, 16440–16446.
- (41) Wachs, I. E.; Weckhuysen, B. M. Structure and Reactivity of Surface Vanadium Oxide Species on Oxide Supports. *Appl. Catal., A* **1997**, *157*, 67–90.
- (42) Kostestky, P.; Yu, J.; Gorte, R. J.; Mpourmpakis, G. Structure–Activity Relationships on Metal-Oxides: Alcohol Dehydration. *Catal. Sci. Technol.* **2014**, *4*, 3861–3869.
- (43) Kostetsky, P.; Mpourmpakis, G. Structure–Activity Relationships in the Production of Olefins from Alcohols and Ethers: a First-Principles Theoretical Study. *Catal. Sci. Technol.* **2015**, *5*, 4547–4555.
- (44) Bell, A. T. The Impact of Nanoscience on Heterogeneous Catalysis. *Science* **2003**, *299*, 1688–1691.
- (45) Calle-Vallejo, F.; Loffreda, D.; Koper, M. T. M.; Sautet, P. Introducing Structural Sensitivity into Adsorption–Energy Scaling Relations by Means of Coordination Numbers. *Nat. Chem.* **2015**, *7*, No. 403.
- (46) Dixit, M.; Kostetsky, P.; Mpourmpakis, G. Structure–Activity Relationships in Alkane Dehydrogenation on γ -Al₂O₃: Site-Dependent Reactions. *ACS Catal.* **2018**, 11570–11578.
- (47) Digne, M.; Sautet, P.; Raybaud, P.; Euzen, P.; Toulhoat, H. Hydroxyl Groups on γ -Alumina Surfaces: A DFT Study. *J. Catal.* **2002**, *211*, 1–5.
- (48) Digne, M.; Sautet, P.; Raybaud, P.; Euzen, P.; Toulhoat, H. Use of DFT to achieve a rational understanding of acid–basic properties of γ -alumina surfaces. *J. Catal.* **2004**, *226*, 54–68.
- (49) Hammer, B.; Norskov, J. K. Theoretical Surface Science and Catalysis—Calculations and Concepts. In *Advances in Catalysis*; Academic Press, 2000; Vol. 45, pp 71–129.
- (50) Suntivich, J.; May, K. J.; Gasteiger, H. A.; Goodenough, J. B.; Shao-Horn, Y. A Perovskite Oxide Optimized for Oxygen Evolution Catalysis from Molecular Orbital Principles. *Science* **2011**, *334*, 1383–1385.
- (51) Fleming, I. *Molecular Orbitals and Organic Chemical Reactions*; John Wiley & Sons Ltd: London, U.K., 2009.
- (52) Jenness, G. R.; Christiansen, M. A.; Caratzoulas, S.; Vlachos, D. G.; Gorte, R. J. Site-Dependent Lewis Acidity of γ -Al₂O₃ and Its Impact on Ethanol Dehydration and Etherification. *J. Phys. Chem. C* **2014**, *118*, 12899–12907.
- (53) Nortier, P.; Fourre, P.; Saad, A. B. M.; Saur, O.; Lavalle, J. C. Effects of crystallinity and morphology on the surface properties of alumina. *Appl. Catal.* **1990**, *61*, 141–160.
- (54) Gribov, E. N.; Zavorotynska, O.; Agostini, G.; Vitillo, J. G.; Ricchiardi, G.; Spoto, G.; Zecchina, A. FTIR spectroscopy and thermodynamics of CO and H₂ adsorbed on γ -, δ - and α -Al₂O₃. *Phys. Chem. Chem. Phys.* **2010**, *12*, 6474–6482.
- (55) Dixit, M.; Kostetsky, P.; Mpourmpakis, G. Structure Activity Relationships in Alkane Dehydrogenation on γ -Al₂O₃: Site-Dependent Reactions. *ACS Catal.* **2018**, *8*, 11570–11578.
- (56) Wang, S.; Petzold, V.; Tripkovic, V.; Kleis, J.; Howalt, J. G.; Skulason, E.; Fernandez, E.; Hvolbæk, B.; Jones, G.; Toftlund, A.; et al. Universal transition state scaling relations for (de) hydrogenation over transition metals. *Phys. Chem. Chem. Phys.* **2011**, *13*, 20760–20765.
- (57) Tsai, C.; Latimer, A. A.; Yoo, J. S.; Studt, F.; Abild-Pedersen, F. Predicting promoter-induced bond activation on solid catalysts using elementary bond orders. *J. Phys. Chem. Lett.* **2015**, *6*, 3670–3674.
- (58) Evans, M.; Polanyi, M. Further considerations on the thermodynamics of chemical equilibria and reaction rates. *Trans. Faraday Soc.* **1936**, *32*, 1333–1360.
- (59) Evans, M.; Polanyi, M. On the introduction of thermodynamic variables into reaction kinetics. *Trans. Faraday Soc.* **1937**, *33*, 448–452.
- (60) Brønsted, J.; Pedersen, K. The catalytic decomposition of nitramide and its physico-chemical applications. *Z. Phys. Chem.* **1924**, *108*, 185–235.
- (61) Hu, C. H.; Chizallet, C.; Mager-Maury, C.; Corral-Valero, M.; Sautet, P.; Toulhoat, H.; Raybaud, P. Modulation of catalyst particle structure upon support hydroxylation: Ab initio insights into Pd13 and Pt13/ γ -Al₂O₃. *J. Catal.* **2010**, *274*, 99–110.

- (62) VandeVondele, J.; Krack, M.; Mohamed, F.; Parrinello, M.; Chassaing, T.; Hutter, J. Quickstep: Fast and accurate density functional calculations using a mixed Gaussian and plane waves approach. *Comput. Phys. Commun.* **2005**, *167*, 103–128.
- (63) Perdew, J. P.; Burke, K.; Ernzerhof, M. Generalized Gradient Approximation Made Simple. *Phys. Rev. Lett.* **1996**, *77*, 3865–3868.
- (64) Grimme, S.; Antony, J.; Ehrlich, S.; Krieg, H. A consistent and accurate ab initio parametrization of density functional dispersion correction (DFT-D) for the 94 elements H-Pu. *J. Chem. Phys.* **2010**, *132*, No. 154104.
- (65) Henkelman, G.; Uberuaga, B. P.; Jonsson, H. A Climbing Image Nudged Elastic Band Method for Finding Saddle Points and Minimum Energy Paths. *J. Chem. Phys.* **2000**, *113* (22), 9901–9904.
- (66) Kresse, G.; Furthmüller, J. Efficient Iterative Schemes for Ab Initio Total-Energy Calculations Using a Plane-Wave Basis Set. *Phys. Rev. B* **1996**, *54*, 11169–11186.
- (67) Kresse, G.; Hafner, J. Ab Initio Molecular Dynamics for Liquid Metals. *Phys. Rev. B* **1993**, *47*, 558–561.
- (68) Kresse, G.; Hafner, J. Ab Initio Molecular-Dynamics Simulation of the Liquid-Metal–Amorphous-Semiconductor Transition in Germanium. *Phys. Rev. B* **1994**, *49*, 14251–14269.